Importance of plasma response to non-axisymmetric perturbations in tokamaks

Jong-kyu Park,[1] Jonathan E. Menard,[1] Allen H. Boozer,[2] Michael J. Schaffer,[3] Andrea M. Garofalo,[3] Stefan P. Gerhardt,[1] Steve A. Sabbagh,[2] Richard J. Hawryluk,[1] Stanley M. Kaye,[1] and the NSTX team[1]

[1]*Princeton Plasma Physics Laboratory, Princeton, New Jersey, NJ 08543*

[2]*Department of Applied Physics and Applied Mathematics, Columbia University, New York, NY 10027*

[3]*General Atomics, San Diego, CA 92186*

(Dated: December 16, 2008)

Abstract

Tokamaks are sensitive to deviations from axisymmetry as small as $\delta B^x/B \sim 10^{-4}$. These non-axisymmetric perturbations greatly modify plasma confinement and performance by either destroying magnetic surfaces with subsequent locking or deforming magnetic surfaces with associated non-ambipolar transport. The Ideal Perturbed Equilibrium Code (IPEC) calculates ideal perturbed equilibria and provides important basis for understanding the sensitivity of tokamak plasmas to perturbations. IPEC calculations indicate the ideal plasma response, or equivalently the effect by perturbed plasma currents is essential to explain locking experiments on NSTX and DIII-D. The ideal plasma response is also important for Neoclassical Toroidal Viscosity (NTV) in non-ambipolar transport. The consistency between NTV theory and magnetic braking experiments on NSTX and DIII-D can be improved when the variation in the field strength in IPEC is coupled with generalized NTV theory. These plasma response effects will be compared with the previous vacuum superpositions to illustrate the importance. Plasma response based on ideal perturbed equilibria, however, can be inconsistent when currents associated with a toroidal torque are comparable to ideally perturbed currents, as briefly discussed with the observation of the expected shielding by torque in NSTX.

I. INTRODUCTION

Tokamaks confine toroidal plasmas to axisymmetric magnetic field, but a small non-axisymmetric field always exists due to the defects of primary magnets. It has been shown that the significant degradation of performance in tokamak plasmas can occur only with non-axisymmetry as small as $\delta B^x/B_0 \sim 10^{-4}$ [1–5]. This is problematic since tokamaks can never be built without such a small error. Interestingly, such a small distortion of tokamak plasmas can be beneficial. Recent experiments on Edge Localized Modes (ELMs) have shown that non-axisymmetry as small as $\delta B^x/B_0 \sim 10^{-4}$ can greatly change ELM behaviors [6–8], which is critical to avoid severe damages by ELMs to plasma-facing components. These observations indicate that tokamaks are very sensitive to small non-axisymmetric perturbations, and thus must be controlled within $\delta B^x/B_0 \sim 10^{-4}$ to improve tokamak plasma performance.

One of standard approximations when describing tokamak plasmas with small non-axisymmetry is to superpose the non-axisymmetric external field $\delta\vec{B}^x$ onto the equilibrium magnetic field $\vec{B}_0$. This approximation essentially assumes that the field $\delta\vec{B}^p$ from perturbed plasma currents is much smaller or at most comparable to the external field $\delta\vec{B}^x$ driven by external currents. The effects by perturbed plasma currents can be designated as plasma response. When the plasma response is considered, the *total field*, $\delta\vec{B} = \delta\vec{B}^x + \delta\vec{B}^p$, can be shielded or amplified with poloidal harmonic coupling, compared to the *external field*, $\delta\vec{B}^x$. The plasma response is essential to understand the sensitivity of tokamaks to small non-axisymmetric perturbations.

The external perturbations in practice change much slower than the relaxation to an equilibrium, so the plasma response can be understood based on three dimensional plasma equilibria. Magnetic surfaces exist everywhere in an axisymmetric tokamak, but non-axisymmetric perturbations can deform or destroy magnetic surfaces. The destruction of magnetic surfaces can occur at the rational surfaces by opening of magnetic islands. When significant islands exist, plasma rotation slows down and can lock to islands [9–12]. Plasma locking must be avoided to maintain good plasma operations. That is, the destruction of magnetic surfaces associated with islands must be negligibly small to maintain plasmas. This is identical to assume ideal evolution of axisymmetric equilibria to non-axisymmetric equilibria since topological changes in magnetic field such as magnetic islands are not al-

lowed in an ideal evolution. Only the deformation of magnetic surfaces can exist by small non-axisymmetric perturbations in ideal perturbed equilibria.

In ideal perturbed equilibria, there are two important consequences [13, 14]: (1) Parallel currents shield the normal resonant field δB_{mn} at the rational surfaces, which determines the property of opening of magnetic islands and thus locking, and (2) the deformation of magnetic surfaces causes non-ambipolar transport due to the symmetry-breaking in $|B|$. In particular, toroidal torque by non-ambipolar transport [15–20] is associated with Neoclassical Toroidal Viscosity (NTV) [21–24]. The two fundamental quantities, δB_{mn} and $|B|$, can be given by ideal perturbed equilibria including plasma response. This paper describes the calculations of ideal perturbed equilibria (Sec. II), brief review of its applications to locking with δB_{mn} (Sec. III), and new applications to NTV torque with $|B|$ (Sec. IV), with comparison with vacuum superpositions to emphasize the importance of ideal plasma response. Plasma response based on ideal perturbed equilibria, however, is not fully self-consistent. Both δB_{mn} and $|B|$ cause a toroidal torque, but currents associated with a toroidal torque is not included in ideal perturbed equilibria. This will be briefly discussed (Sec. V) with followed by summary and future work (Sec. VI).

II. IDEAL PERTURBED EQUILIBRIUM CODE

The Ideal Perturbed Equilibrium Code (IPEC) [25], based on DCON [26] and VACUUM [27] stability codes, solves free-boundary perturbed equilibria preserving the pressure $p(\psi)$ and the safety factor $q(\psi)$ profiles specified by a given axisymmetric equilibrium. The fixed $q(\psi)$ profile means that any topological change of magnetic field lines is not allowed and thus that magnetic islands are suppressed. Mathematically, IPEC solves the perturbed force balance

$$\vec{F}[\vec{\xi}] = \vec{0} = \vec{\nabla}\delta p - \delta\vec{j} \times \vec{B}_0 - \vec{j}_0 \times \delta\vec{B}, \tag{1}$$

with the internal boundary conditions at the $q = m/n$ rational surfaces,

$$\Phi_{mn} = 0 = \frac{1}{(2\pi)^2} \oint d\vartheta \oint d\varphi \mathcal{J} \delta\vec{B} \cdot \vec{\nabla}\psi e^{-i(m\vartheta - n\varphi)}. \tag{2}$$

This internal boundary condition suppresses the magnetic islands at the rational surfaces. The external boundary conditions are given by $\delta\vec{B}^x \cdot \hat{n}_b$ on a control surface, or equivalently on the plasma boundary. As detailed description in Ref. [25], the self-consistent normal

field on the plasma boundary is determined by $\delta\vec{B}\cdot\hat{n}_b = \overleftrightarrow{P}[\delta\vec{B}^x\cdot\hat{n}_b]$ with a permeability operator. IPEC uses virtual surface currents to construct the permeability operator, so initially gives the self-consistent field only inside the plasma. It is not difficult to construct the self-consistent field outside the plasma if the vacuum field from coils is given, but this is not discussed in this paper.

The internal boundary condition ensures that there is no magnetic island at the rational surfaces. Instead, magnetic islands are shielded by parallel currents flowing at the rational surfaces. The total resonant field δB_{mn} is the field canceled by the shielding currents, otherwise would arise and open magnetic islands. The shielding currents at the rational surfaces are important part of ideal plasma response, or equivalently perturbed plasma currents.

Perturbed plasma currents including shielding currents at the rational surfaces can greatly modify the penetration of the field. This can be easily illustrated with a cylindrical and force-free ($p = 0$) plasma with a non-axisymmetric perturbation. Suppose a cylindrical plasma with the $q = 2$ resonant surface at $r/a \sim 0.8$ inside with the minor radius $r = a$. The plasma is enclosed by a conformal thin wall located $r/a = 1.2$. When $(m = 2, n = 1)$ external currents exist at the wall, free boundary perturbed equilibrium can be solved easily in vacuum, and also in plasma with a simple numerical routine using Cylinder force-free equation. In this limit, the perturbed magnetic field can be written as $\delta\vec{B} = \vec{\nabla}\delta A_\parallel \times \hat{z} = \hat{r}(1/r)(\partial\delta A_\parallel/\partial\theta) - \hat{z}(\partial\delta A_\parallel/\partial r)$. With a perturbation $\delta A_\parallel = \delta A_\parallel \cos(m\theta - n\phi)$, the perturbed equilibrium can be given by [28]

$$\frac{1}{r}\frac{d}{dr}\left(r\frac{d\delta A_\parallel}{dr}\right) - \frac{m^2\delta A_\parallel}{r^2} = \frac{q}{r}\frac{m}{m-nq}\frac{d}{dr}(KR_0)\delta A_\parallel, \tag{3}$$

given a current profile $KR_0(r) = (R_0/B_0)\mu_0 j_\parallel(r)$.

Fig. 1 shows the solutions by vacuum superposition and Cylinder force-free equation. For comparison, IPEC solution is also shown for a near cylindrical ($\epsilon = 0.1$) and near force-free ($\beta_N = 0.1$) example. One can see that IPEC solution using virtual surface currents is almost identical to Cylinder force-free solution inside the plasma. The benchmark of IPEC solution in the cylindrical limit has been done in this way. Compared to vacuum superpositions, the ideally perturbed equilibrium (by either of IPEC or Cylinder force-free solution) shows a fundamental difference. The normal field is completely shielded inside the resonant surface and the jump in the derivative of normal field implies currents shielding

the normal resonant field. Also, there are significant plasma currents outside the resonant surface as well to change the profile of the normal field. As a result, one can find strong shielding of the field inside the plasma, compared to vacuum superposition.

The amplification also can be easily found in the cylindrical force-free example. Fig. 2 shows free boundary solutions by vacuum superposition, Cylinder force-free, and IPEC as in Fig. 2, for $(m = 3, n = 1)$ external current at the wall. This amplification arises since $q = 3$ surface is close to and outside the plasma boundary, so the energy required to perturb plasma is very small as well known in ideal MHD theory [29].

In tokamak plasmas with significant toroidicity, poloidal harmonic coupling is also very strong in addition to shielding and amplification. Therefore, plasma responses, or equivalently perturbed plasma currents, predominantly determine perturbed field and displacement. Vacuum superposition not only can give incorrect evaluation of the perturbed quantities, but also can give misleading physics. The finite resonant field at the rational surfaces in vacuum superposition will destroy every rational surfaces, which is not true in normal tokamak operations due to perturbed plasma currents.

III. DESTRUCTION OF FLUX SURFACES AND PLASMA LOCKING

Plasma locking occurs if shielding currents can not be maintained and thus magnetic islands open at the rational surfaces. There is the critical amplitude of perturbations, over which the balance is lost between viscous torque by rotation and electromagnetic torque by shielding currents. This is often called *field penetration* [9–12]. The balance is determined by the inner-layer dynamics, but shielding currents must be determined by perturbed equilibria. IPEC gives shielding currents before the onset of locking, when magnetic islands can be ignored and thus ideal perturbed equilibria can be used.

IPEC applications to plasma locking problems have highlighted the importance of plasma response [30]. In both NSTX [31] and DIII-D [32] experiments, each set of particular experiments was not consistent with the previous observations when the external resonant field δB^x_{mn} was used. The previous observations have shown that locking density is approximately proportional to the amplitude of the external field [1–5]. If the spectrum of the external field is fixed in a set of experiments, the resonant field must be proportional to an amplitude of the external field independently of a component of the external field used for specifying

the amplitude. If the spectra become different by various combinations of intrinsic error and correction field, one must specify a component of external field to estimate a resonant field driving magnetic islands. The failure to acquire a positive correlation between the locking density and the external resonant field implies that the external resonant field does not represent properly a driving resonant field for locking.

The difference between the external resonant field and the total resonant field should be clarified. From Fig. 1, for instance, one can read the external resonant field $\delta B^x_{21} \sim 0.8 Gauss$ approximately at the $q = 2$ surface. However, the resonant field including plasma response (IPEC or Cylinder force-free) is suppressed since parallel currents completely shield out the resonant field driving magnetic islands. That is, the resonant field driving magnetic islands must be evaluated from the shielding currents $\vec{j}_s$, by $\vec{\nabla} \times \delta\vec{B} = \mu_0 \vec{j}_s$. In this way, the total resonant field in Fig. 1 is $\delta B_{21} \sim 0.5 Gauss$ which would arise when the shielding currents $\vec{j}_s$ are all dissipated. The previous picture by the external resonant field is supposed to approximate this picture by the total resonant field, but has been often misleadingly taken as the existence of the finite external resonant field and of magnetic islands, which are not true before a locking occurs.

In toroidal geometry with a finite pressure, the difference between the external resonant field and the total resonant field can become very large. Fig. 3 shows the results NSTX and DIII-D locking experiments, in terms of the resonant field versus density at locking. Fig. 3 (b) data are the same as Ref. [30], but here magnetic coordinates with ordinary toroidal angles (called PEST) are used for all the resonant field instead of Hamada coordinates. As noted in Ref. [33], the resonant field depends on magnetic coordinates and the approximations are valid only for core region where the torodicity is not so strong. The external resonant field in NSTX may be able to approximate the total resonant field, but it can be greatly misleading as can be seen for DIII-D. DIII-D has more diverse spectra of non-axisymmetric field than NSTX due to two more rows of coils at the off-midplane. Even if the external resonant field is almost canceled by corrections at a rational surface, the total resonant field can remain very large due to irrelevancy of vacuum approximation in tokamak plasmas.

IV. DEFORMATION OF FLUX SURFACES AND NTV TRANSPORT

Deformed magnetic surfaces distort trajectories of particle orbits and produce so-called non-ambipolar transport [15–20], since the transport is different for species. Ions typically diffuse faster, and resulting net radial currents produce toroidal torques until ambipolar electric field is restored. Therefore, non-ambipolar transport causes rotational damping, and the associated viscosity is often called Neoclassical Toroidal Viscosity (NTV) [21–24]. One can use non-axisymmetric field to change toroidal rotation and this is called NTV magnetic braking [34, 35] of rotation in experiments.

A. Variation of field strength

There are various theoretical predictions for NTV that can be compared with experimental damping rates of rotation. Any of evaluations needs information of $B = |B|$ and thus requires the calculations of perturbed equilibria. This can be easily understood by considering the action of a trapped particle with given energy H and magnetic moment μ as

$$J = \oint v_{\|} dl \propto \oint \sqrt{H - \mu |B|} dl. \tag{4}$$

The action must be conserved for a particle, but the action is dependent on toroidal location in the presence of the non-axisymmetry in $|B|$. Hence, a particle must drift radially to conserve the action while precesses toroidally.

It should be emphasized that the non-axisymmetry in B must be evaluated along the true magnetic field lines dl. That is, non-axisymmetric variations in B, δB, must be evaluated along perturbed magnetic field lines. This *Lagrangian* evaluation for the variation in the field strength is given by [14]

$$\delta_L B = \delta_E B + \vec{\xi} \cdot \vec{\nabla} B_0, \tag{5}$$

in the lowest order of the perturbation and the *Eulerian* evaluation at fixed points in space is

$$\delta_E B = \delta \vec{B} \cdot \hat{b}, \tag{6}$$

where $\hat{b} = \vec{B}_0 / B_0$ is the unit vector of the unperturbed magnetic field. Note that the variation of field strength in Eulerian frame is determined by tangential components of

perturbed magnetic field. The vacuum approximation for the variation in the field strength uses the external field instead of the total field, that is,

$$\delta_E B^x = \delta\vec{B}^x \cdot \hat{b}. \tag{7}$$

The difference of two Eulerian evaluations, $\delta_E B$ and $\delta_E B^x$, depends on plasma response. However, the correct variation in the field strength for Eq. (4) is not either of them, but is the Lagrangian evaluation in Eq. (5). The Lagrangian $\delta_L B$ is typically larger than Eulerian evaluation since it is dominantly determined by spatial variations of $B_0 \propto 1/R$, which is much larger than perturbed field δB, seen in $\vec{\xi}$ displaced magnetic field lines. The example is shown in Fig. 4, where $n = 1$ field using Error Field (EF) coils with a typical current $\sim 1kA$ is applied to a NSTX plasma. A moderate $\beta_N = 1.0$ is chosen to suppress large amplifications as one can see from that $\delta_E B$ is similar to vacuum approximation $\delta_E B^x$. Although plasma amplifications can be ignored, one can see that the Lagrangian evaluation is larger than vacuum approximation by an order of magnitude. In practice, vacuum approximation gives $\delta_E B^x/B_0 \sim 10^{-4}$ and Lagrangian evaluation including plasma response gives $\delta_L B/B_0 \sim 10^{-3}$ except the applied field is close to a marginally stable mode. Since NTV transport is proportional to $\delta_L B^2_{mn}$ for a single harmonic perturbation, this difference can give $\sim 10^2$ factors in the calculations.

The Lagrangian $\delta_L B$ in IPEC can provide relevant prediction for the variation in the field strength, however, the singularity exists in the narrow region around the rational surfaces. This arises because the tangential displacement is determined by $\vec{\nabla} \cdot \vec{\xi} = 0$ and gives $\xi_\parallel \propto \vec{\nabla} \cdot \vec{\xi}_\perp/(m - nq)$. This is the feature of ideally perturbed equilibria and can remain if only the evaluation for a local torque is desired. However, the regularization is required for the evaluation for the total toroidal torque. IPEC alters the tangential displacement as [29]

$$\xi_\parallel \propto \frac{m - nq}{(m - nq)^2 + \sigma^2} \vec{\nabla} \cdot \vec{\xi}_\perp, \tag{8}$$

with a small parameter σ, which can be reasonably taken as an ion gyro-radius $\Delta_g \psi$ and corresponding $\sigma \approx (m - n\Delta_g q)$. The integration and the total torque are not sensitive to variations of σ, if $\sigma \sim \sigma_g$ within an order of magnitude, since only the very narrow region around the rational surfaces is affected by the regularization. Despite the regularization, the peaks around the rational surfaces as seen in Fig. 4 may be still nonphysical. This is in fact the consequence of non-self-consistency in ideally perturbed equilibria, which will be discussed in Sec. V.

B. Theoretical prediction of NTV braking

The variation in the field strength $\delta_L B$ given by IPEC can be used to evaluate NTV torques and rotational damping rates. NTV transport has been studied by a number of authors. In particular, Shaing has calculated various asymptotic limits in perturbed tokamaks including multi-harmonic perturbations [21–24]. It has been known that there are two main regimes, the $1/\nu$ regime [23] when $\omega_E << \nu$ and the $\nu_{-}\sqrt{\nu}$ regime [24] when $\omega_E >> \nu$. Although the calculations are more realistic than the previous calculations with a single harmonic perturbation, it is still difficult to apply the results to tokamaks since the regimes overlap, and the transport in different regimes differs by several orders of magnitude. Also, the precession rates are sufficiently strong for NBI-heated tokamaks to give resonances with bounce of trapped particles. Therefore, a generalized formula has been derived to include precessions and resonant effects and to combine different regimes [20]. The resonant effects between the electric precession and the bouncing orbits have been calculated by Ref. [19] for a single harmonic perturbation, but the new generalization includes multi-harmonic perturbations, magnetic precession, and combines different regimes using an effective collisional operator. Including the general formula, here two evaluations in the asymptotic limits, in the $1/\nu$ regime and in the $\nu_{-}\sqrt{\nu}$ regime, are also summarized for comparison.

The results can be written for a flux-averaged toroidal force density, $\tau_\varphi \equiv \vec{\tau} \cdot (\partial \vec{x}/\partial \varphi) \equiv \langle \hat{\phi} \cdot \vec{\nabla} \cdot \overleftrightarrow{\Pi}_a \rangle$ for species a, where $\hat{\phi}$ is the unit vector of ordinary toroidal angle. Dropping the species a subscripts, each evaluation gives

$$\tau_{\varphi,1/\nu} = \frac{\epsilon^{3/2} p u^{\varphi}_{1/\nu}}{\sqrt{2}\pi^{3/2}} \left\langle \frac{1}{R} \right\rangle \frac{1}{\nu} \int_0^1 d\kappa^2 \delta^2_{w,1/\nu} \tag{9}$$

$$\tau_{\varphi,\nu_{-}\sqrt{\nu}} = \frac{\epsilon^{-1/2} p u^{\varphi}_{\nu_{-}\sqrt{\nu}}}{\sqrt{2}\pi^{3/2}} \left\langle \frac{1}{R} \right\rangle \frac{1}{\omega_E^2} \int_0^1 d\kappa^2 \delta^2_{w,\nu_{-}\sqrt{\nu}} \tag{10}$$

$$\tau_{\varphi,\ell} = \frac{\epsilon^{1/2} p u^{\varphi}_{\ell}}{\sqrt{2}\pi^{3/2}} \left\langle \frac{1}{R} \right\rangle \int_0^1 d\kappa^2 \delta^2_{w,\ell} \int_0^\infty dx \mathcal{R}_{1,\ell}, \tag{11}$$

for $1/\nu$, $\nu_{-}\sqrt{\nu}$ and general formula, respectively. The ϵ is the inverse aspect ratio, p is the pressure of species, R is the major radius, ω_E is the toroidal precession angular frequency. The δ^2_w is the square of variation in the field strength with different weighting factor for

different harmonic perturbations.

$$\delta^2_{w,1/\nu} \equiv \sum_{nmm'} \delta^2_{nmm'} \frac{n^2 F^{1/2}_{nm0} F^{1/2}_{nm'0}}{E(\kappa) - (1-\kappa^2)K(\kappa)} \tag{12}$$

$$\delta^2_{w,\nu\text{-}\sqrt{\nu}} \equiv \sum_{nmm'} \delta^2_{nmm'} (E(\kappa) - (1-\kappa^2)K(\kappa)) \tag{13}$$

$$\times \left(\frac{\partial L_{nmc}}{\partial \kappa^2} \frac{\partial L_{nm'c}}{\partial \kappa^2} + \frac{\partial L_{nms}}{\partial \kappa^2} \frac{\partial L_{nm's}}{\partial \kappa^2} \right) \tag{14}$$

$$\delta^2_{w,\ell} \equiv \sum_{nmm'} \delta^2_{nmm'} \frac{n^2 F^{-1/2}_{nm\ell} F^{-1/2}_{nm'\ell}}{4K(\kappa)}, \tag{15}$$

where $K(\kappa)$ is the elliptic integral of the first kind, $E(\kappa)$ of the second kind and

$$\delta^2_{nmm'} = Re(\delta_{nm}) Re(\delta_{nm'}) + Im(\delta_{nm}) Im(\delta_{nm'}). \tag{16}$$

Each function is defined as

$$F^y_{nm\ell} \equiv \int_{-\vartheta_t}^{\vartheta_t} (\kappa^2 - \sin^2(\vartheta/2))^y \cos(m - nq - \sigma\ell)\vartheta \tag{17}$$

$$L_{nmc} \equiv \frac{F^{-1/2}_{nm0}}{2K(\kappa)} \left(1 - \cos(\sqrt{n}\varsigma) e^{-\sqrt{n}\varsigma} \right) \tag{18}$$

$$L_{nms} \equiv \frac{F^{-1/2}_{nm0}}{2K(\kappa)} \left(\sin(\sqrt{n}\varsigma) e^{-\sqrt{n}\varsigma} \right), \tag{19}$$

with the turning point $\vartheta_t \equiv 2\arcsin(\kappa)$, the sign function that $+1$ for co-rotating case, and the stretch variable related to the width of layer for $\sqrt{\nu}$ regime as [24]

$$\varsigma = (1-\kappa^2) \left(\frac{\ln(16/\sqrt{4\nu/\epsilon\omega_E})}{4\nu/\epsilon\omega_E} \right)^{1/2}. \tag{20}$$

The resonant term in Eq. (11) is given by

$$\mathcal{R}_{1,\ell} = \frac{1}{2} \frac{(1 + (\frac{\ell}{2})^2) \frac{\nu}{2\epsilon} x e^{-x}}{(\ell\omega_b - n(\omega_E + \omega_B))^2 + \left((1 + (\frac{\ell}{2})^2) \frac{\nu}{2\epsilon} \right)^2 x^{-3}}. \tag{21}$$

The bounce frequency ω_b and the magnetic precession ω_B are functions of (x, κ^2), but one can use further approximations as functions only of x. The approximations are

$$\omega_b = \frac{\pi\sqrt{\epsilon}}{2\sqrt{2}} \omega_t \frac{\sqrt{x}}{K(\kappa)} \approx \frac{\pi\sqrt{\epsilon}}{4\sqrt{2}} \omega_t \sqrt{x}, \tag{22}$$

$$\omega_B = \sigma \frac{q^3 \omega_t^2}{2\epsilon\omega_g} x \frac{F^{-1/2}_{010}(\kappa)}{4K(\kappa)} \approx \sigma \frac{q^3\omega_t^2}{4\epsilon\omega_g} x, \tag{23}$$

where the transit frequency $\omega_t = v_t/qR_0$ and the gyrofrequency $\omega_g = eB/M$.

The torque is proportional to the toroidal flow $u^\varphi = \vec{u}\cdot\vec{\nabla}\varphi$ with an offset by the neoclassical flow as

$$u_N^\varphi \equiv u^\varphi + C_N \sigma \left| \frac{1}{e}\frac{dT}{d\chi} \right|. \tag{24}$$

For each regime, $C_{1/\nu} \approx 3.5$, $C_{\nu\text{-}\sqrt{\nu}} \approx 0.92$, and $C_\ell \approx 2.0$.

The Eqs. (9) $\sim$ (24) can be used for comparison with experiments, but these formulas have limitations : (1) The evaluations take only the trapped particles into account. The effects by passing particles are expected to be weaker than trapped particles. This can be seen by comparing the $1/\nu$ evaluation for trapped particles and the collisional [21] or plateau [36] evaluations for passing particles [35], ignoring precessions or resonances. However, a systematic evaluation for passing particles with the precessions has not been resolved yet. (2) The radial excursions of banana orbits from a magnetic surface are ignored, which can drive complicated effects involved in the variations of the electric potential. (3) The field model ignores high-order shaping terms of plasmas assuming a high aspect-ratio circular tokamak. Although the model can describe effectively the width and the depth of magnetic wells, present tokamaks typically have strong shaping and so NTV evaluations can be inaccurate especially in the edge. Also, (4) the analytic treatments cannot exactly describe complicated interactions between precessions, particle orbits and collisions in the presence of multi-harmonic perturbations, which can lead stochastic transport [17]. These limitations have to be resolved by numerical evaluations, for instance, using δf code, in the future.

C. Experimental measurement of NTV braking

The Eqs. (9) $\sim$ (24) gives various evaluations for toroidal torque, which can be compared with experiments. While making comparison between theory and experiment, it is convenient to use rotational damping rates as

$$\nu_{damp} \cong \frac{\tau_\varphi}{u_\varphi R_0 M N}, \tag{25}$$

where M is the mass and N is the density of a species.

Fig. 5. shows $n = 3$ magnetic braking experiments performed in NSTX. The two shots have almost identical plasma, run in lower single null configuration, elongated as high as $\kappa = 2.3$, with $I_p = 800kA$ (Fig. 5 (a)) and $B_{T0} = 0.45T$. The electron densities are similar to each other (Fig. 5 (b)), although the slow evolutions imply that kinetic equilibria

need longer time scale. For one of these shots, $n = 3$ braking field is applied using RWM coils in NSTX with currents $600A$ for each (Fig. 5 (c)). One can see from (b) that the amplitude of the braking is low enough not to change particle confinement, and also not to change heat confinement. A clear change was made in the momentum confinement. The plasma rotation reached up to $20 \sim 30kHz$ in the early period by $6MW$ NBI and settled down to similar rotational equilibrium as shown in Fig. 5 (d). However, when the braking field is fully applied at $t = 500ms$, the toroidal rotation starts to damp and relaxes to a different rotational equilibrium. This example indicates the non-ambipolar transport by non-axisymmetric field can produce a strong momentum transport, but the particle and heat transport can be dominated by neoclassical ambipolar or anomalous transport. Also, the use of a reference shot as in these examples is important to discriminate the effects by the non-ambipolar transport.

The change of toroidal rotation is determined not only by the non-ambipolar transport with perturbations, but also by various sources including the turbulence-driven momentum transport [37] and the input torque by NBI. The momentum balance equation can be written as

$$MN\frac{\partial \Omega}{\partial t} = \langle \hat{\phi} \cdot \delta \vec{j} \times \delta \vec{B} \rangle - \langle \hat{\phi} \cdot \vec{\nabla} \cdot \overleftrightarrow{\Pi} \rangle \tag{26}$$

$$+ \frac{\partial}{\partial \rho}\left(MN\chi_\phi \frac{\partial \Omega}{\partial \rho} - MNV^{pinch}\Omega \right) + S, \tag{27}$$

for the time evolution. This is a symbolic form representing each relevant physics. The first term in the right hand side is the torque arising at the rational surfaces due to the shielding currents, and is related to locking property in the Sec III. The second term is the non-ambipolar torque related to magnetic braking. The third term includes a diffusive process of the transport and a pinch, both of which can include classical, neoclassical and turbulence driven momentum transport. The last term represents the source by the additional heating, mainly by NBI. The best way to discriminate the second term in experiments is to use a reference shot that can be subtracted from a magnetic braking shot. The plasma condition must be almost identical, and one must determine the damping in a short time period, otherwise the different rotation evolution can make differences for other terms in Eq. (27). When the time period is short enough, the exponential decay of the rotation to a new rotational equilibrium can be linearized. In NSTX, the experimental rotational damping rates are measured in this way. The time period is as short as $\sim 50ms$, beyond which the

linear behavior can not be assumed.

Fig. 6 shows the evolutions of the rotation mapped on the flux surfaces, with and without $n = 3$ magnetic braking. One can see the profile of the toroidal rotation is almost identical right before the magnetic braking ($t = 500ms$), but evolves differently after the magnetic braking, so one can subtract (a) from (b) to obtain the damping purely driven by the braking. This example is in fact better since the rotation does not evolve very much during the period of time considered. This settlement of the rotation in an equilibrium, however, is not seen for all the cases, and it is necessary to use an identical reference shot.

There are other issues in the comparison with the observed damping rates. The toroidal rotation in NSTX (and DIII-D) is measured by CHarge Exchange Recombination Spectroscopy (CHERS) based on Carbon impurity. Here it will be assumed that the CHERS measurement represents the toroidal rotation of the main ions, as commonly assumed in other experiments. However, since a certain amount of time is required to achieve the equilibration between carbon ions and main (deuterium) ions, a damping seen by CHERS can have more smooth profile than the immediate response of the main ions. These are ignored in our study, but must be addressed in the future.

D. Comparison between theory and experiment

The measured damping rates purely by the magnetic braking can be compared with the calculations of NTV using IPEC field. There has been different methods, for instance, using a separate regime and only the external field, which have been quite successful to approximate the observed damping rates in NSTX [35]. Here three additional physics are included to improve the consistency further :

(a) Toroidal precession rates ($\omega_p = \omega_E + \omega_B$) are often faster than the collisional rates (ν).

(b) The bouncing orbits of trapped particles can resonate with the precessions, that is, $\ell\omega_b \sim n\omega_p$.

(c) Variation of field strength along the perturbed magnetic field lines, that is, $\delta_L B$, including plasma response is substantially different from vacuum approximation $\delta_E B^x$.

As in the Fig. 7, one can obtain different evaluations if

(1) (a), (b) and (c) are all ignored : vacuum $1/\nu$

(2) (a) is only included : vacuum $1/\nu\_\nu$

(3) (a) and (b) are included : vacuum general

(4) (a), (b) and (c) are all included : IPEC general

The evaluation assuming $1/\nu$ regime based on vacuum approximation can be close to measurement (vacuum $1/\nu$), but in presence of the strong precession, the prediction becomes too small (vacuum $1/\nu\_\nu$) unless the bounce-harmonic resonances (vacuum general) and simultaneously the true variation in the field strength are considered (IPEC general).

The example shown in Fig. 7 even follows the complicated profile of damping rates very well. However, this is not for all the cases. Fig. 8 showed comparisons of the damping rates between measurements and NTV calculations, in NSTX and DIII-D, respectively. As one can see, predictions are valid only within an order of magnitude, but generally fails to follow the detailed profiles in the measurements. Generally, the measured damping rates are much smoother than the predictions. Among many possible reasons for these deviations in both theory and experiment as described, the non-self-consistency in ideal perturbed equilibria is probably most important.

V. NON-SELF-CONSISTENCY IN IDEAL PLASMA RESPONSE

When the variations in the field strength are calculated using IPEC and are used for the calculations of a toroidal torque, the inconsistency occurs since scalar pressure perturbed equilibria $\vec{\nabla}p = \vec{j} \times \vec{B}$ have no toroidal torque. The toroidal torque is given by a tensor pressure $\vec{\nabla} \cdot \overleftrightarrow{\Pi}$. If a toroidal torque evaluated in IPEC is comparable to a perturbed scalar pressure energy, one needs to solve tensor pressure perturbed equilibria, $\vec{\nabla}p + \vec{\nabla} \cdot \overleftrightarrow{\Pi} = \vec{j} \times \vec{B}$ [38]. Note the torque and the energy have the same units. There is no proper method yet to compare the detailed profiles of the two in a self-consistent way. However, it is possible to compare the total energy with the total torque for plasma since the integration of tensor pressure perturbed equilibria over the whole volume of plasma gives a relation between the total values and external magnetic measurements [39].

The external magnetic measurements can determine

$$s \equiv -\frac{\delta W}{\delta W_v} \text{ and } \alpha \equiv -\frac{T_\varphi}{2\delta W_v}, \tag{28}$$

where δW is the total perturbed energy, δW_v is the energy required to make the same perturbations in vacuum, and T_φ is the total toroidal torque, that is, the volume integration of τ_φ in Eqs. (9) $\sim$ (11). When $|s| >> |\alpha|$, ideal perturbed equilibria can be a good approximation, but when $|s| \sim |\alpha|$, the energy and the torque evaluated by IPEC would be inconsistent. In particular, the currents associated with the torque would shield external perturbations since it becomes difficult for the perturbation to tap the energy from plasma due to a toroidal phase shift [39].

Fig. 9 shows a set of NSTX experiments with $n = 1$ rotating external field [39]. The (s_E, α_E) are the experimentally derived values from magnetic sensors, and the (s_T, α_T) are the evaluations using IPEC and generalized NTV in Eq. (11). One can see that the inconsistency occurs between experiment (s_E, α_E) and theory (s_T, α_T) when $|s_E| \sim |\alpha_E|$ and $|s_T| \gtrsim |\alpha_T|$. The study implies that tensor pressures are more important for higher β_N, especially above the no wall limit $\beta_N \sim 4.0$. Also, one can see the expected shielding from $\alpha_E < \alpha_T$ in high β_N.

The higher n perturbations have the higher no-wall limit in terms of β_N, and $|s| >> |\alpha|$ for most of practical applications. For instance, all the $n = 3$ applications studied in Figs. (7) $\sim$ (8) have $|s| > 0.5$ and $|\alpha| < 0.2$ for NSTX, and $|s| > 0.8$ and $|\alpha| < 0.1$ for DIII-D, indicating the relevancy of ideal perturbed equilibria. However, tensor pressure equilibria are necessary for any case to improve the detailed profiles of perturbation and torque. As discussed already, the singularity in $\xi_\parallel$ and the peaks in Fig. 4 indicate the very large toroidal torque around the rational surfaces, which would not be physical and would be shielded by local tensor pressures.

VI. SUMMARY AND FUTURE WORK

The characteristics of perturbed tokamak equilibria and the importance of ideal plasma response are illustrated. The Ideal Perturbed Equilibrium Code (IPEC) solves perturbed tokamak equilibria only with deformed magnetic surfaces suppressing magnetic islands. IPEC has shown that the effects by perturbed plasma currents can make not only dif-

ferent penetration of the field, but also strong shielding and amplification in general. The IPEC applications to locking experiments in both NSTX and DIII-D have highlighted the importance of plasma response in perturbed tokamaks. The inconsistency of the external resonant field explaining the critical locking density has been resolved by the total resonant field driving magnetic islands that can be obtained from IPEC calculations. The total resonant field will be used to construct global locking scaling between devices to predict the locking threshold in ITER.

The importance of plasma response effects is also illustrated in the non-axisymmetric variation of the field strength, which causes non-ambipolar transport and NTV braking of toroidal rotation. The actual variation in the field strength evaluated along perturbed magnetic field lines is different and typically larger than Eulerian evaluation along the unperturbed magnetic field lines in vacuum or including plasma response. When the IPEC variation in the field strength is coupled with generalized theory of non-ambipolar transport, the consistency between experiment and theory can be improved. However, there are still various unresolved issues in both experiment and theory. Especially IPEC equilibria have no toroidal torque, and thus the extension of IPEC to tensor pressure perturbed equilibria is important to be fully self-consistent in the description of the field strength, associated NTV braking and non-ambipolar transport.

This work was supported by DOE contract DE-AC02-76CH03073 (PPPL), DE-FG02-03ERS496 (CU) and DE-FC02-04ER54698 (GA).

---

[1] T. C. Hender, R. Fitzpatrick, A. W. Morris, P. G. Carolan, R. D. Durst, T. Eddlington, J. Ferreira, S. J. Fielding, P. S. Haynes, J. Hugill, et al., Nucl. Fusion **32**, 2091 (1992).

[2] R. J. La Haye, R. Fitzpatrick, T. C. Hender, A. W. Morris, J. T. Scoville, and T. N. Todd, Phys. Fluids B **4**, 2098 (1992).

[3] R. J. Buttery, M. D. Benedetti, D. Gates, Y. Gribov, T. Hender, R. La Haye, P. Leahy, J. Leuer, A. Morris, A. Santagiustina, et al. (1999).

[4] J. T. Scoville and R. J. LaHaye, Nucl. Fusion **43**, 250 (2003).

[5] J. E. Menard, M. G. Bell, R. E. Bell, E. D. Fredrickson, D. A. Gates, S. M. Kaye, B. P. LeBlanc, R. Maingi, D. Mueller, S. A. Sabbagh, et al., Nucl. Fusion **43**, 330 (2003).

[6] T. E. Evans, R. A. Moyer, P. R. Thomas, J. G. Watkins, T. H. Osborne, J. A. Boedo, E. J. Doyle, M. E. Fenstermacher, K. H. Finken, R. J. Groebner, et al., Phys. Rev. Lett. **92**, 235003 (2004).

[7] T. E. Evans, R. A. Moyer, J. G. Watkins, T. H. Osborne, P. R. Thomas, M. Becoulet, J. A. Boedo, E. J. Doyle, M. E. Fenstermacher, K. H. Finken, et al., Nucl. Fusion **45**, 595 (2005).

[8] R. A. Moyer, T. E. Evans, T. H. Osborne, P. R. Thomas, M. Becoulet, J. H. Harris, K.-H. Finken, J. A. Boedo, E. J. Doyle, M. E. Fenstermacher, et al., Nucl. Fusion **43**, 330 (2003).

[9] R. Fitzpatrick, Nucl. Fusion **33**, 1049 (1993).

[10] A. Cole and R. Fitzpatrick, Phys. Plasmas **13**, 032503 (2006).

[11] A. Cole, C. C. Hegna, and J. D. Callen, Phys. Rev. Lett. **99**, 065001 (2007).

[12] R. Fitzpatrick and T. C. Hender, Phys. Fluids B **3**, 645 (1991).

[13] A. H. Boozer and C. Nührenberg, Phys. Plasmas **13**, 102501 (2006).

[14] A. H. Boozer, Phys. Plasmas **13**, 044501 (2006).

[15] E. A. Frieman, Phys. Fluids **13**, 490 (1970).

[16] A. A. Galeev, R. Z. Sagdeev, H. P. Furth, and M. N. Rosenbluth, Phys. Rev. Lett. **22**, 511 (1969).

[17] R. J. Goldston, R. B. White, and A. H. Boozer, Phys. Rev. Lett. **47**, 647 (1981).

[18] R. Linsker and A. H. Boozer, Phys. Fluids **25**, 143 (1982).

[19] H. E. Mynick, Nucl. Fusion **26**, 491 (1986).

[20] J.-K. Park, A. H. Boozer, and J. E. Menard, Phys. Rev. Lett. (2009), submitted.

[21] K. C. Shaing, Phys. Fluids **26**, 3315 (1983).

[22] K. C. Shaing, Phys. Rev. Lett. **87**, 245003 (2001).

[23] K. C. Shaing, Phys. Plasmas **10**, 1443 (2003).

[24] K. C. Shaing, P. Cahyna, M. Becoulet, J.-K. Park, S. A. Sabbagh, and M. S. Chu, Phys. Plasmas **15**, 082506 (2008).

[25] J.-K. Park, A. H. Boozer, and A. H. Glasser, Phys. Plasmas **14**, 052110 (2007).

[26] A. H. Glasser and M. S. Chance, Bull. Am. Phys. Soc. (1997).

[27] M. S. Chance, Phys. Plasmas **4**, 2161 (1997).

[28] A. H. Boozer, Rev. Mod. Phys. **78**, 1071 (2005).

[29] J. P. Freidberg, *Ideal Magnetohydrodynamics* (Plenum Press, New York, 1993).

[30] J.-K. Park, M. J. Schaffer, J. E. Menard, and A. H. Boozer, Phys. Rev. Lett. **99**, 195003

(2007).

[31] M. Ono, S. Kaye, Y.-K. Peng, G. Barnes, W. Blanchard, M. Carter, J. Chrzanowski, L. Dudek, R. Ewig, D. Gates, et al., Nucl. Fusion **40**, 557 (2000).

[32] J. L. Luxon and L. G. Davis, Fusion Technology **8**, 441 (1985).

[33] J.-K. Park, A. H. Boozer, and J. E. Menard, Phys. Plasmas **15**, 064501 (2008).

[34] A. M. Garofalo, K. H. Burrell, J. C. Deboo, J. S. deGrassie, G. L. Jackson, M. Lanctot, H. Reimerdes, M. J. Schaffer, W. M. Solomon, E. J. Strait, et al., Phys. Rev. Lett. **101**, 195005 (2008).

[35] W. Zhu, S. A. Sabbagh, R. E. Bell, J. M. Bialek, B. P. LeBlanc, S. M. Kaye, F. M. Levinton, J. E. Menard, K. C. Shaing, A. C. Sontag, et al., Phys. Rev. Lett. **96**, 225002 (2006).

[36] K. C. Shaing, S. P. Hirshman, and J. D. Callen, Phys. Fluids **29**, 521 (1986).

[37] W. M. Solomon, S. M. Kaye, R. E. Bell, B. P. LeBlanc, J. E. Menard, G. Rewoldt, and W. Wang, Phys. Rev. Lett. **101**, 065004 (2008).

[38] A. H. Boozer, Phys. Rev. Lett. **86**, 5059 (2001).

[39] J.-K. Park, A. H. Boozer, J. E. Menard, S. P. Gerhardt, and S. A. Sabbagh, Phys. Plasmas (2009), submitted.

List of Figures

Figures

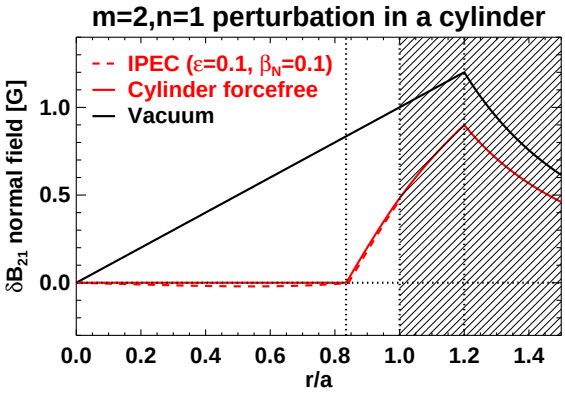

FIG. 1: The normal field δB_{21} as a function of the radius in a perturbed cylindrical force-free plasma. Each solution is obtained using vacuum superposition (Vacuum), Cylinder force-free equation (Cylinder force-free), and IPEC with virtual surface currents (IPEC). Cylinder force-free and IPEC give the almost identical solution for plasma and show strong shielding inside the resonant surface $q = 2/1$.

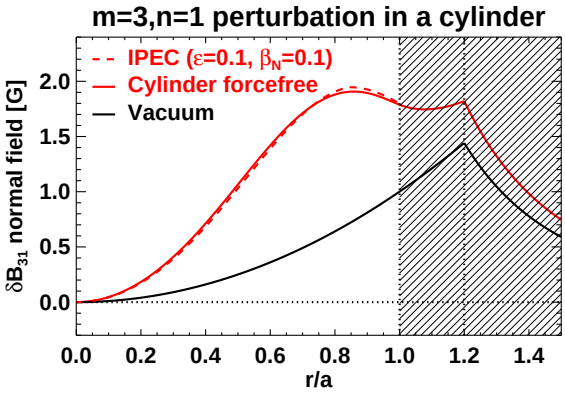

FIG. 2: The normal field δB_{31} as a function of the radius in a perturbed cylindrical force-free plasma. As Fig. 1, each solution is obtained using vacuum superposition (Vacuum), Cylinder force-free equation (Cylinder force-free), and IPEC with virtual surface currents (IPEC). Cylinder force-free and IPEC give the almost identical solution for plasma and show strong amplification throughout plasma.

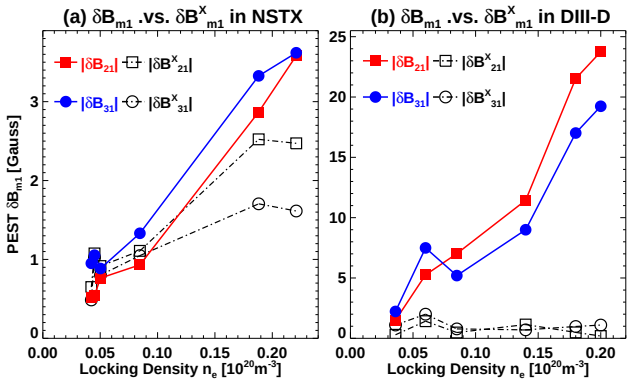

FIG. 3: The critical amplitude of the resonant field versus density at locking in (a) NSTX and (b) DIII-D experiments. The external resonant field δB^x_{mn} is compared with the total resonant field δB_{mn} at $q = 2/1$ and $q = 3/1$ rational surfaces. PEST means specific magnetic coordinates using the ordinary toroidal angle. Linear correlation between the total resonant field and locking density can be seen in both NSTX and DIII-D.

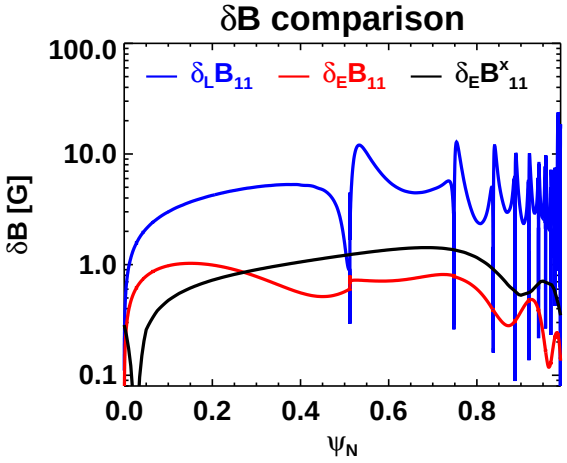

FIG. 4: Comparison for the radial profiles of one component (m=1,n=1) of the non-axisymmetric variation in the field strength between Eulerian vacuum ($\delta_E B^x$), Eulerian IPEC ($\delta_E B$) and Lagrangian IPEC ($\delta_L B$) evaluations. The calculation is done with a typical $n = 1$ Error Field (EF) coil current ($\sim 1kA$) to a moderate $\beta_N = 1.0$ NSTX plasma, so plasma amplifications are not strong in this example. However, Lagrangian evaluation is still larger than other two Eulerian evaluations.

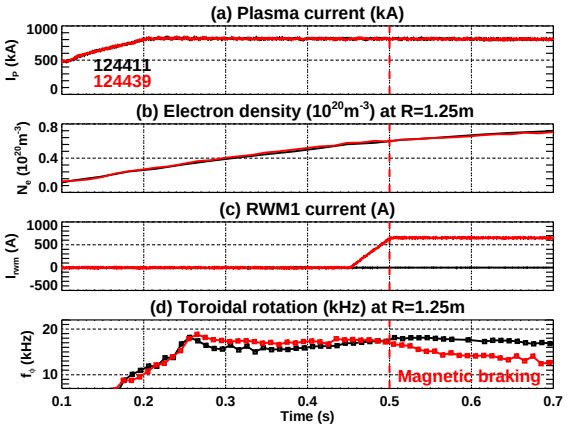

FIG. 5: Magnetic braking experiments in NSTX. Time evolutions for (a) Plasma current, (b) Electron density, (c) n=3 RWM current, and (d) Toroidal rotation are shown for plasmas with (red) and without (black) magnetic braking.

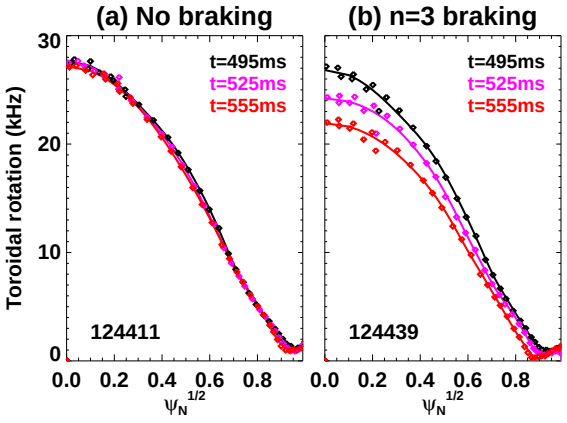

FIG. 6: Comparison of the evolution of the rotational profile mapped on the flux surfaces (a) without a magnetic braking and (b) with $n = 3$ magnetic braking as shown in Fig. 5 (b)

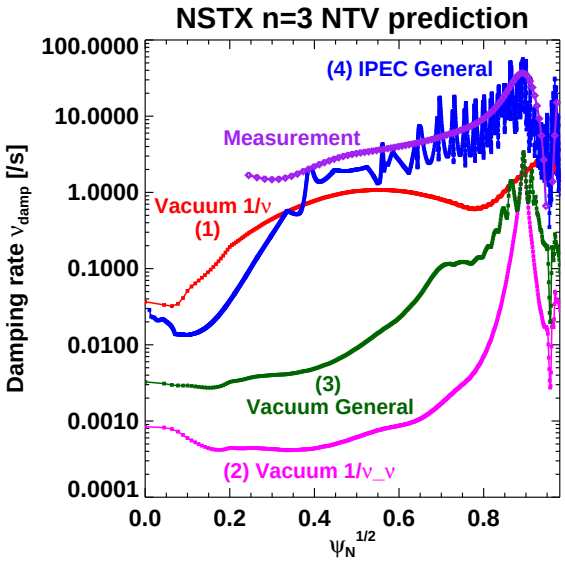

FIG. 7: Comparisons between measured damping rates (NSTX #124439.00500) and different methods of NTV calculations. (1) $1/\nu$ evaluation using Eq. (9) and vacuum field ($\delta_E B^x$), (2) $\nu_-\sqrt{\nu}$ evaluation using Eq. (10) and vacuum field, (3) general evaluation using Eq. (11) and vacuum field, and (4) general evaluation using IPEC field ($\delta_L B$).

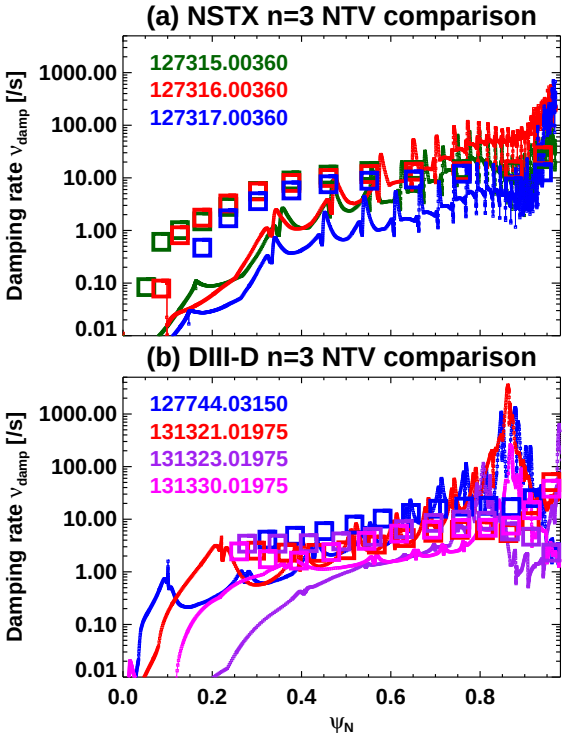

FIG. 8: Comparisons of the damping rates as functions of ψ_N between measurements (□) and general IPEC NTV calculations in (a) NSTX and (b) DIII-D .

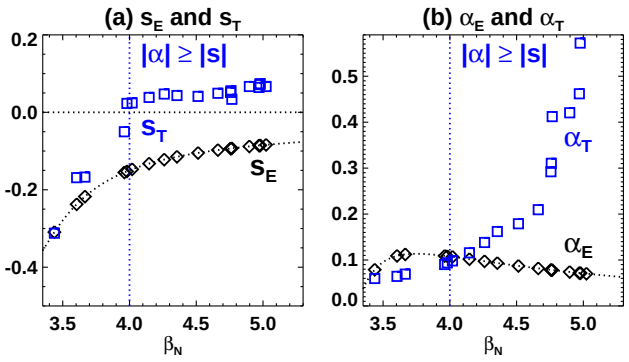

FIG. 9: Ref. [39]. Comparison (a) between averaged s_T (blue) and s_E (black), and (b) α_T (blue) and α_E (black). Note the good agreement between the measurement and the theory when $|\alpha| < |s|$, but the inconsistency occurs when $|\alpha| \geq |s|$ since the currents associated with the torque are not included in ideally perturbed equilibria. It can be seen the additional (a) stabilizing effect in s_E and (b) shielding effect in α_E by the torque.